Row and column artifacts in JWST MIRI's Si:As blocked impurity band detectors

Daniel Dicken, George Rieke, Michael Ressler, Jane Morrison, Macarena Garcia Marin, et al.

Published version information:

Citation: D Dicken et al. Row and column artefacts in JWST MIRI's Si:As blocked impurity band detectors. In Space Telescopes and Instrumentation 2022: Optical, Infrared, and Millimeter Wave, Montréal, Canada, 17-23 Jul 2022, (2021): 103.

DOI: 10.1117/12.2630027

PROCEEDINGS OF SPIE

SPIEDigitalLibrary.org/conference-proceedings-of-spie

Row and column artifacts in JWST MIRI's Si:As blocked impurity band detectors

Daniel Dicken, George Rieke, Michael Ressler, Jane Morrison, Macarena Garcia Marin, et al.

Daniel Dicken, George Rieke, Michael Ressler, Jane Morrison, Macarena Garcia Marin, Ioannis Argyriou, Karl D. Gordon, Mike Regan, Christophe Cossou, Andras Gaspar, Alistair Glasse, Pierre Guillard, Alvaro Labiano, Gillian Wright, "Row and column artifacts in JWST MIRI's Si:As blocked impurity band detectors," Proc. SPIE 12180, Space Telescopes and Instrumentation 2022: Optical, Infrared, and Millimeter Wave, 121802R (27 August 2022); doi: 10.1117/12.2630027

SPIE.

Event: SPIE Astronomical Telescopes + Instrumentation, 2022, Montréal, Québec, Canada

Row and column artifacts in JWST MIRI's Si:As blocked impurity band detectors

Daniel Dicken[a,*], George Rieke[d], Mike Ressler[e], Jane Morrison[b,d], Macarena Garcia Marin[b], Ioannis Argyriou[f], Karl D. Gordon[b], Mike Regan[b], Christophe Cossou[c], Andras Gaspar[d], Alistair Glasse[a], Pierre Guillard[g], Alvaro Labiano[h,i], Gillian Wright[a]

[a]UK Astronomy Technology Centre, Royal Observatory Edinburgh, Blackford Hill, Edinburgh EH9 3HJ, UK
[b]Space Telescope Science Institute, 3700 San Martin, Drive, Baltimore, MD, 21218, USA
[c]AIM, CEA, CNRS, Universite Paris-Saclay, Universite Paris Diderot, Sorbonne Paris Cite,F-91191 Gif-sur-Yvette, France
[d]Steward Observatory, University of Arizona, Tucson, AZ 85721, USA
[e]Jet Propulsion Laboratory, California Institute of Technology, 4800 Oak Grove Drive, Pasadena, CA 91109, USA
[f]Instituut voor Sterrenkunde, KU Leuven, Celestijnenlaan 200D, bus-2410, 3000 Leuven, Belgium
[g]Sorbonne Universiteé, CNRS, UMR 7095, Institut d'Astrophysique de Paris, 98bis bd Arago, 75014 Paris, France
[h]Telespazio UK for the European Space Agency, ESAC, Camino Bajo del Castillo s/n, 28692 Villanueva de la Cañada, Spain.
[i]Centro de Astrobiología (CSIC-INTA), Carretera de Ajalvir, 28850 Torrejón de Ardoz, Madrid, Spain.

Abstract.
The JWST Mid-Infrared Instrument (MIRI) detector arrays are Si:As blocked impurity band devices, direct descendants of the Spitzer/IRAC long wavelength arrays. Similarly to the IRAC row-column effect, analysis of flight-like MIRI detector data has shown that columns and rows in which source signals are located can suffer from pull up (brightness increase) or pull down (brightness decrease) in the flux image. Here we present results from the JPL MIRI detector characterisation campaigns dedicated to understanding this row-column effect as well as the first results showing the effect in the flight detectors for MIRI. We show the effect is flux dependent and confirm that the effect manifests differently for rows versus columns. We discuss the origin of the flux offset, which is related to a change in the signal output in time that distorts the input ramp as a function of the saturation level of illuminated pixels. We conclude by discussing the row-column effect in the context of different MIRI instrument modes and present preliminary proposals to mitigate and/or correct the effect in MIRI data.

Keywords: detectors, infrared, JWST , MIRI.

*Daniel Dicken, daniel.dicken@stfc.ac.uk

1 Introduction

The JWST Mid-Infrared Instrument (MIRI) detector arrays are arsenic-doped impurity band conduction (IBC) devices, supplied by Raytheon Vision Systens and direct descendants of the Spitzer/IRAC long wavelength arrays - Channels 3 and 4.[1,2] These are the detectors of choice for space applications between 5 and 28 microns, with relatively high quantum efficiencies (7-12 microns >55%, 12-27 microns >60%), low dark currents ($\sim$ 0.2 e-/s) and resistance to the detrimental effects of

Space Telescopes and Instrumentation 2022: Optical, Infrared, and Millimeter Wave, edited by Laura E. Coyle, Shuji Matsuura, Marshall D. Perrin, Proc. of SPIE Vol. 12180, 121802R · © 2022 SPIE · 0277-786X · doi: 10.1117/12.2630027

cosmic ray impacts. Similar devices were also used in WISE,[3] MSX,[4] and Akari,[5] although the MIRI devices are closest in heritage to the Spitzer/IRAC arrays.

Despite their outstanding performance, the required low temperature of operation ($\sim$ 6 - 7 K) affects the electronic properties of these detector arrays in ways that require careful calibration to remove artifacts. To improve our understanding of the MIRI detectors, we conducted an extensive series of cryogenic pre-flight detector test campaigns at the NASA Jet Propulsion Laboratory (JPL). One of the issues addressed in these tests was an artifact in which a bright source on the detector is seen to pull up or pull down the flux value in the entire rows and columns that the source is observed in. This artifact also reported for the Spitzer IRAC detectors, Channels 3 and 4.[6,7] artifacts of a related nature are seen in the Spitzer IRS and MIPS silicon IBC arrays (supplied by Boeing North America), described as a "jailbar" effect (see MIPS Instrument Handbook), a pattern across the entire array that emerges after the multiplexing moves past a saturated region. Similarly, IRAC Channels 1 and 2 used the same readout as Channels 3 and 4, operated at a different temperature, and saw a related set of artifacts (described in the IRAC Instrument Handbook[1]). The presence of related, but different in detail, artifacts in these three array types, covering two different multiplexers and detector types (Si:As, In:Sb), confirms that the artifacts originate in the multiplexer rather than in the detector layers. In all cases, they probably arise through some combination of overdriving on-chip electronics with long recovery time constants, and electronic crosstalk.

This paper describes a series of tests to help characterise the row-column effect further in the MIRI detectors. As a starting point that defines the type of issues, the IRAC handbook (Section 7.2.4) describes column pull-down/pull-up occurring for very bright sources or cosmic ray hits.

[1] https://irsa.ipac.caltech.edu/data/SPITZER/docs/irac/iracinstrumenthandbook/

It resulted at an approximate signal level of 35000 DN[2], which then produced a change in signal intensity along the columns that the source was detected in. The effect did not scale linearly with flux but was equal on either side of the point of origin. The Spitzer IRAC tests did not find a specific *row* pull-down/pull-up effect in their Si:As detectors. However, this behavior might have been masked by what we define as the cruciform artifact[8] in MIRI data. The cruciform arises due to diffraction effects within the detector (slit diffraction at the narrow gaps between pixel physical boundaries) and extends in both rows and columns, described as "banding" by the IRAC team.

An important distinction between the Spitzer IRAC read-out data and MIRI data is that with MIRI we downlink samples along the entire integration ramp, whereas Spitzer only sent down the measured slope of the ramp. This means that row and column artifacts could only be investigated in flux space for Spitzer. For MIRI, we can investigate the effect at the level of individual frames, which proves to be important in our understanding. For this reason we do not refer to the effect as a pull-up or pull-down because whether the flux change is positive or negative depends on the length of ramp and the level of flux for the source or origin, as we will show. Therefore in this paper we refer to the effect as simply row-column artifacts.

The paper is organised as follows. First we present the pre-flight test results from our NASA JPL test campaigns, describing and characterising the effects. Next we show the artifacts in MIRI flight data and discuss the impact on the science mission for MIRI. Finally we look to the future and the possibility of corrections and mitigation for row and column artifacts in MIRI data.

[2]Digital Numbers (equivalent to Analog-to-Digital Units

2 Initial characterisation of the effect in NASA JPL ground testing

An investigation of the row-column artifact was undertaken at NASA JPL from 2016 through 2021 in a series of cryo-vacuum test campaigns. The tests at NASA JPL used engineering model detectors that are nearly identical to the flight detectors except for packaging. These were used in the development of the flight arrays. The JPL tests also included flight-like focal plane electronics (FPE)[2] so overall the detector and FPE system was very close to what could be expected from the flight system. The detectors were mounted inside a cryo-vacuum module to put them at their operating temperature of 6.4K. The investigation into the row-column effect was made by illuminating the detectors with a blackbody source filtered at 15 microns. To create sources falling on the detector plane a mask plate was placed over the detector array, with three holes representing a bright point source, a faint point source and a semi-extended source (disc).

Figure 1 shows the resulting flux image constructed from the detector integration slopes[3], measured viewing the masked black body for an incident flux of approximately 400 DN/s. The detector readout was set to FAST[4] and this example uses one integration with 40 groups, i.e., a total integration of 111 seconds. The left image in Figure 1, with a linear scale, shows the two ”point” sources and the disk from the mask. On the right is the same image but with a stretched background to show the column and row artifacts, manifested as a pull-up or pull-down in flux of the detector rows and columns illuminated by the bright test sources.

The amplitude of these row and column artifacts is very small. In this example from a relatively bright source, the artifacts deviated from the background signal by no more than a few tenths of

[3]JWST data including MIRI uses the MULTIACCUM readouts also known as ”sample up the ramp” described in the JWST documentation here https://jwst-docs.stsci.edu/understanding-exposure-times.

[4]FAST is equivalent to FASTR1 that is the default readout mode for MIRI flight data, but FAST includes only one rather than two resets between subsequent integrations. Both modes sample up the integration ramp at 2.775 second intervals, each of which is termed a “group.”

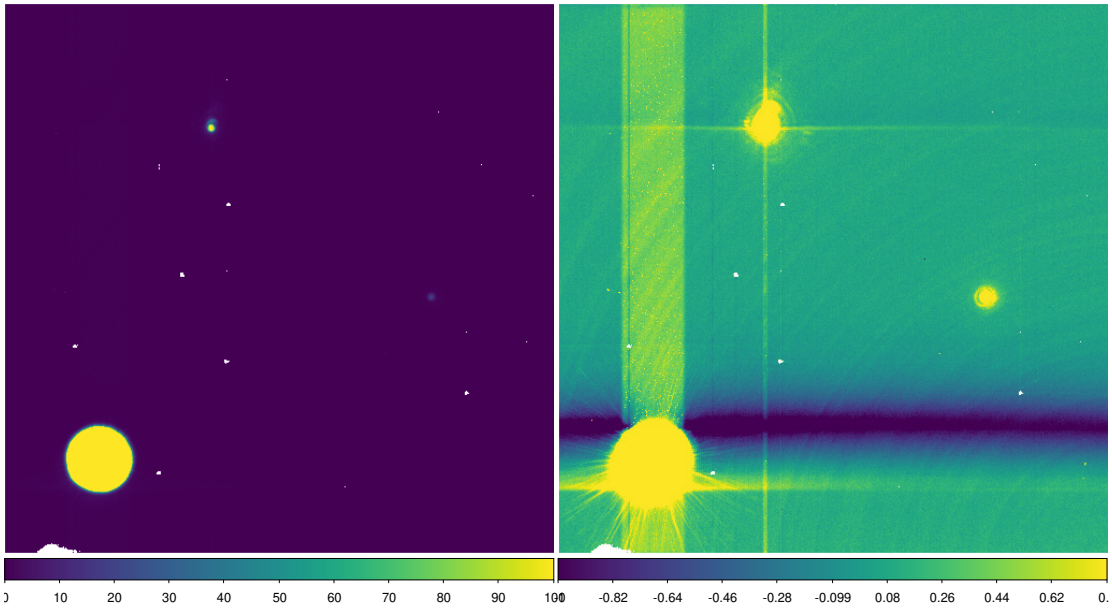

Fig 1 Figure showing slope images from the JPL ground test campaign. Left: a linear scale image showing the two point sources and the disk from the masked black body source. Right: the same image but with the background stretched to reveal the column and row artifacts. White spots on the image are hot or bad pixels on these detectors. In flight these pixels are flagged by the pipeline and mitigated through multiple imaging while dithering.

a DN/s in flux. However, for the sensitivity of JWST MIRI, this level of detector artifact can be important. There is also no row-column artifact from the fainter of the two point sources in the test. This gives us an initial indication that the artifact is flux dependent and probably more important for bright sources.

To show the influence of the column artifact on the background of the test images in Figure 2 we show a row profile (red line through image) of a row of pixels without sources. The plot shows the results for four different flux levels, 40, 80, 200 and 400 DN/s, from the test source. We can see that the two brighter sources from the masked black body affect the background for columns in which the sources are located. The number of columns affected coincides well with the size of the source and also the column effect increases with flux. However, we stress the effect is still small, $\sim$0.2 DN/s change in the background for a source signal of 400 DN/s. For reference the highest flux that MIRI could theoretically observe with a minimum 2 frames in full-array is approximately

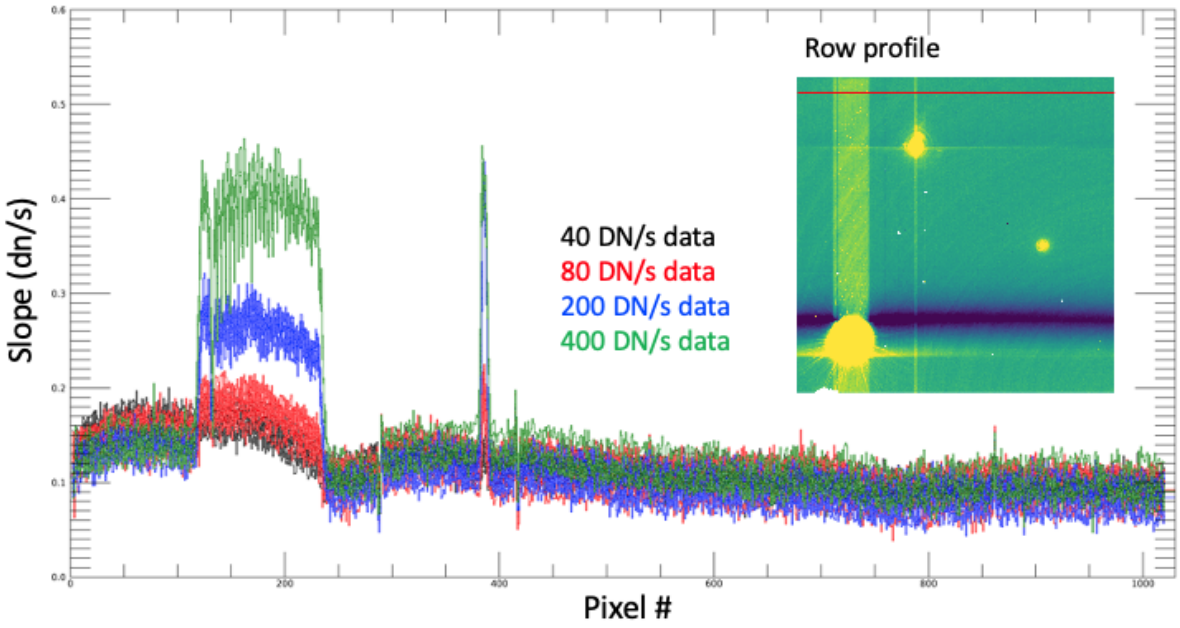

Fig 2 Showing the column artifact profiles in a flux image. The row profiles for four different flux levels are plotted, which correspond to the profile as represented by the red line in the inset image.

28,000 DN/s.

To show the row effect in Figure 3 we show a column profile, again for a column without test sources, marked as a red line in the image in the figure. Here we see that rows illuminated by the extended disk source are pulled up for rows at the bottom of the source image and pulled down at the top of the source image. Contrary to the column artifact, the row artifact extends beyond the rows that include source images, especially for the more extended disc-like test source. This initial investigation also indicates that the number of affected rows and the intensity of the row artifact appears to be related to the source size, rather than its intensity.

The initial investigation also showed that the row and column artifacts are to first order constant in amplitude across the detector in either the row or column direction. There is some evidence of a row dependence for very bright sources where the effect is fractionally stronger when measured closer to the source of origin.

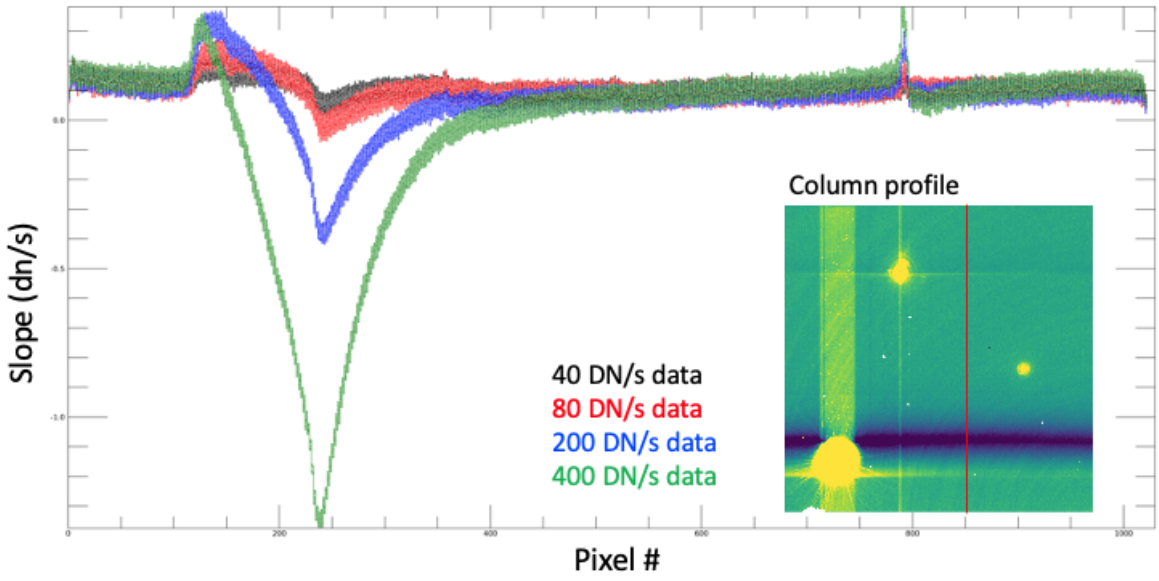

Fig 3 Showing the row artifact profiles in a flux image. The profiles for four different flux levels are plotted, which correspond to the profile as represented by the red line in the inset image.

It is also noteworthy that Figures 2 and 3 show that the strength of the effect does not seem strongly dependent on the number of illuminated row and column pixels; i.e., one might expect for the disk test source that the rows and columns at the edge of the disk, which have less illuminated pixels per row or column, would show less column and row pull down, but this is not the case, to first order. The absolute flux on the pixels seems to be more dominant in the effect than the number of pixels illuminated in any row or column.

Figure 4 shows many images from the JPL test with increasing flux of the source. The row and column effects can clearly be seen to increase with flux in these slope images. What is apparent in Figure 4 is that the row and column effect can be seen at all flux levels down to 5 DN/s (albeit at very low contrast). This is particularly true for the disk source, as also found in previous investigations. That is, the effect is not limited to bright source data as suggested from Spitzer IRAC data. Again it is important to note that the row and column effects will appear enhanced in the JPL ground test data, which has particularly low backgrounds compared to flight imager data – a factor

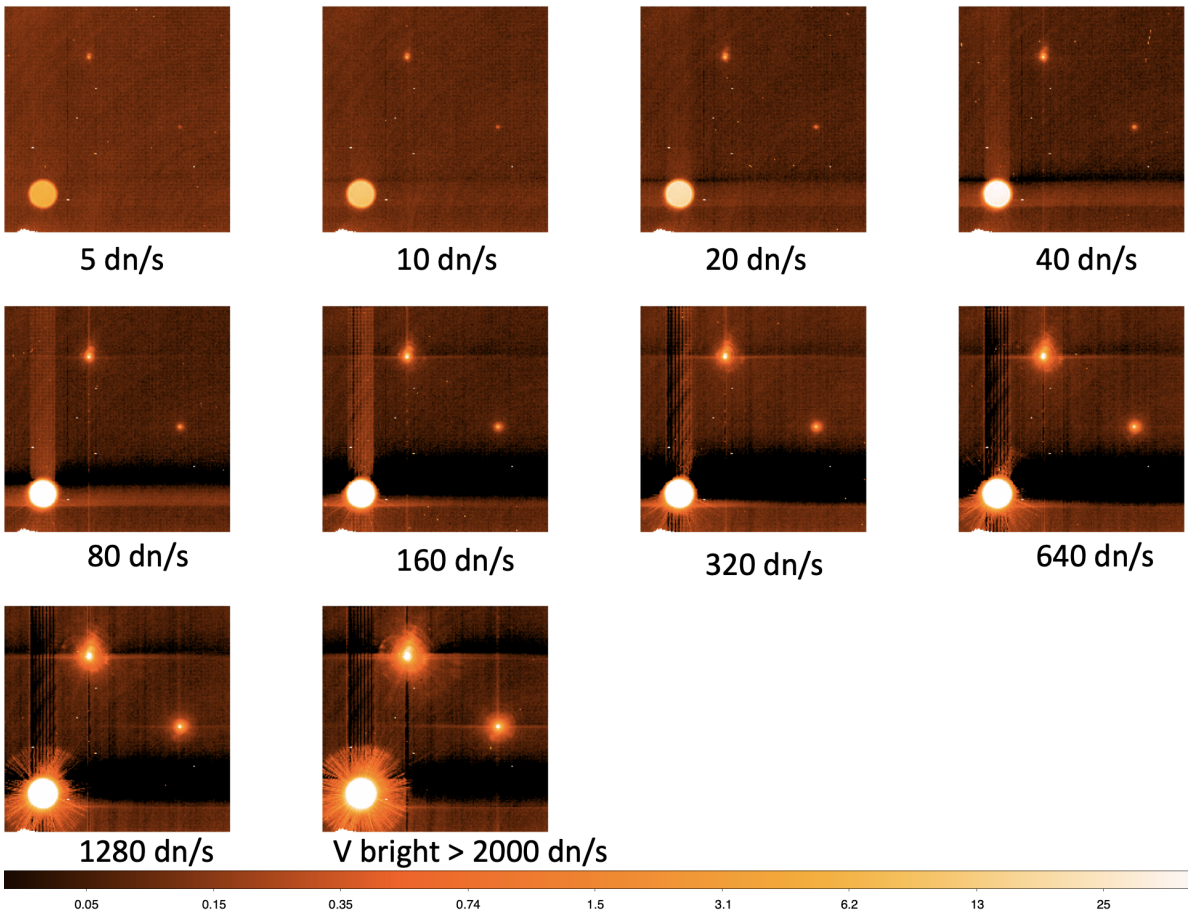

Fig 4 Showing flux images from NASA JPL test bench. The row-column artifact can be seen to have a stronger influence as the flux of the source increases.

of 3 lower than our lowest backgrounds at 5.6 micron for MIRI imaging.

2.1 Origin of the row column effect

JPL test results show that the origin of the artifact in slope images is a complex set of influences on the slopes themselves related *both* to the brightness of the source causing the effect *and* to the time to saturation in the ramp. To show the origin of the row-column artifact in slope images we then need to investigate the ramps under different conditions.

To do so, we will study the individual frame images that are fit to create the slope or flux image. In Figure 5 we again show the row-column artifact image from JPL testing but with three regions

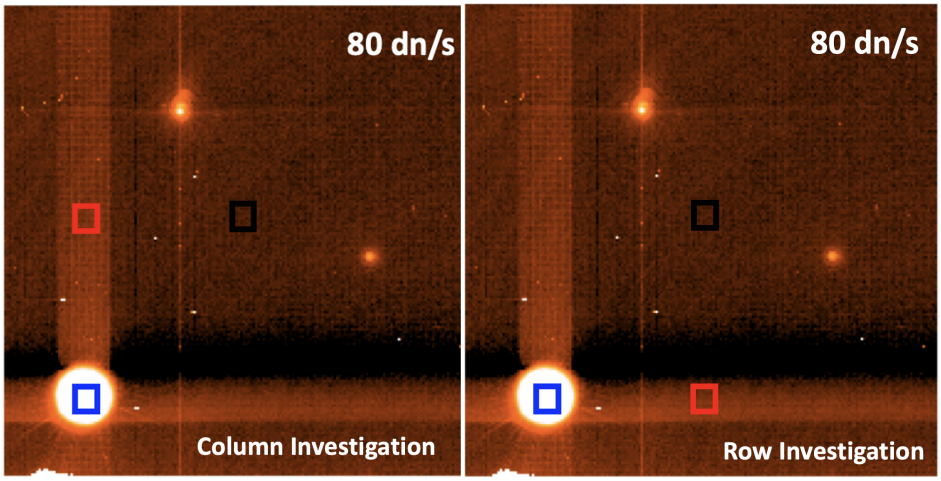

Fig 5 Showing the flux image from the JPL test bench. The three boxes mark regions used in the following investigation. The black box marks a region used as a reference background. The red box marks a region used to investigate an area with row or column artifacts. The blue box represents a region on the JPL test source image itself. The disk source is used in the following investigation

marked with boxes. The following investigation shows the mean signal per frame for these three boxed regions: (1) the blue box on the source, (2) the red box on the row or column artifact and (3) the black box on a region without sources or row-column artifacts as a reference. Figure 6 shows the ramp results for the column artifact for four flux levels in separate plots, 80, 160, 320, 640 DN/s. The black points in the plots show the signal per frame in the ramp for the reference boxed region not affected by the column artifact. We can see that the ramps for these reference regions do not change for the four flux levels investigated. The red data points in the figure represent the signal per frame measured in the red box region with the column artifact. Here we see that as the flux of the source increases with each test, the red ramp data are increasingly distorted compared to the reference ramp. Finally, in the inset plot, we plot the ramps of the source signal. A close inspection of Figure 6 shows when the signal from the source (shown by the blue points of the inset plot) reaches saturation, the slope of the ramp for the column artifact pixels becomes negative.

Next, Figure 7 investigates the signal in the ramps of the row artifact. Presented in an identical

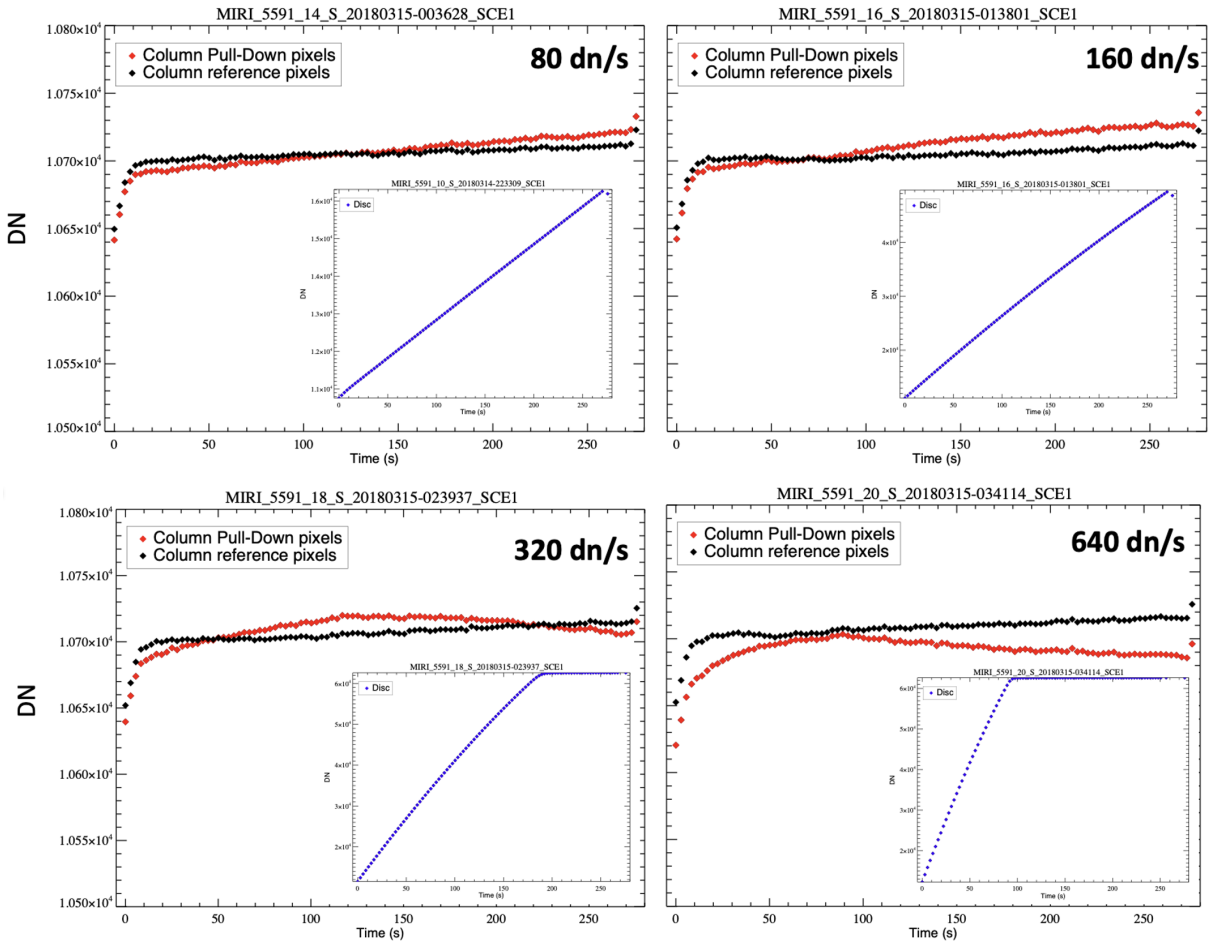

Fig 6 Showing four plots, each one for a different flux level in the JPL test, where the source flux was set to 80, 160, 320 and 640 DN/s. The detector outputs are color-coded to match the color of the relevant box in Figure 5. The black points represent the signal measured from an individual frame of the ramp in the reference region as defined in Figure 5. The red points represent the same measurement per frame for the column artifact region. The blue points show the signal from the disk test source itself.

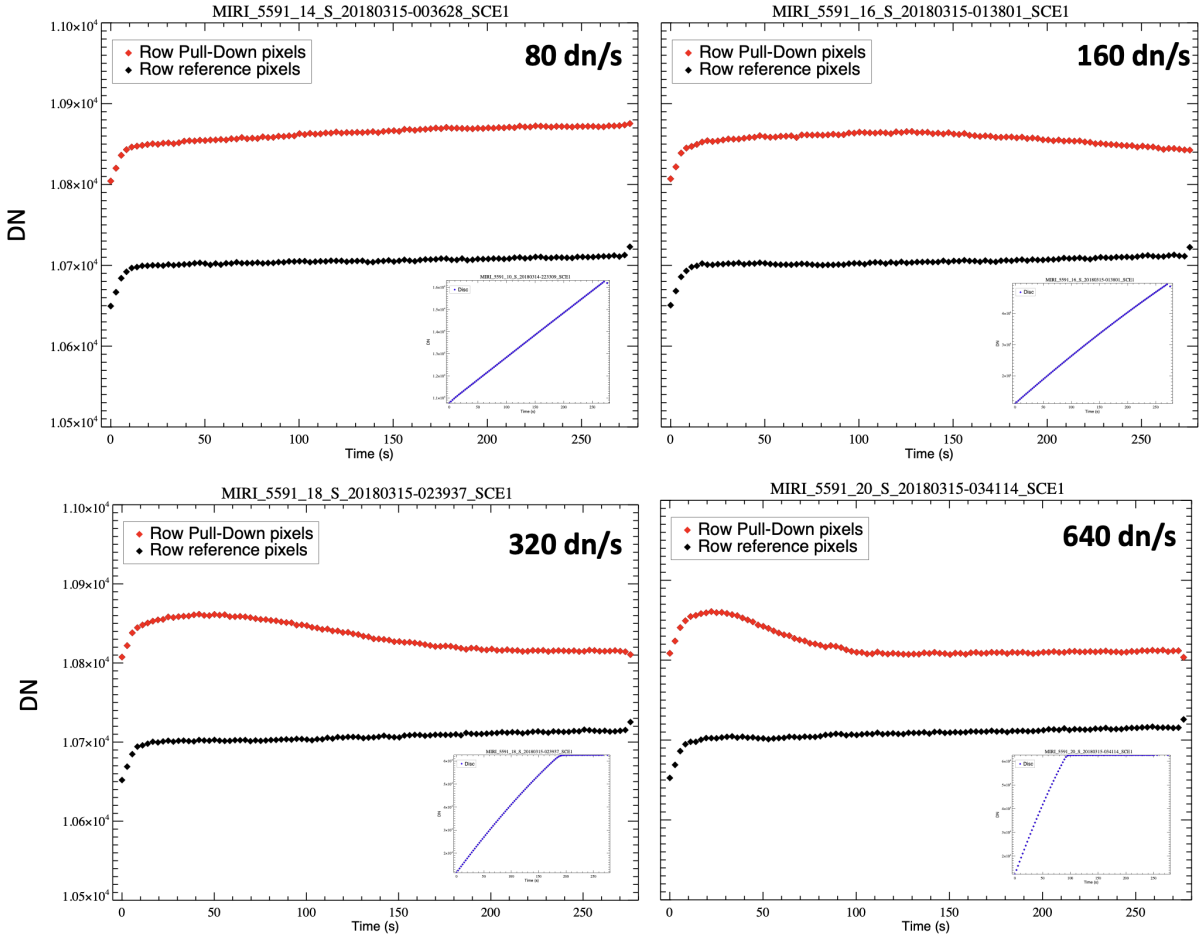

Fig 7 Same as for Figure 6 but the red points here show the signal in individual frames or the ramp for the row artifact.

way to Figure 6 we can immediately see that row artifact ramps (red points) are distorted compared with the reference background ramp (black points). Again we show the signal of the ramps of the disk source per frame as an inset plot. With careful inspection of Figure 7 we see that when the signal saturates in the ramp, the distortion in the row effect is reduced. That is to say that when the signal saturates, it appears that there is little or no row effect on the background ramp frames. This is different from the column effect and is the first indication that the row and column effects are non-identical and perhaps have different origins.

To show the lack of row effect after saturation more clearly, in Figure 8 we plot similar results for very bright test source data. The figure shows the reference and the row artifact ramps for fluxes of 1280 DN/s and "very bright" where the latter is the maximum flux of the ground test source. The bottom two plots in Figure 8 show the ramps of the source saturating in the disk in 50 seconds and 25 seconds for the two flux levels respectively. The top two plots show the corresponding box fit for ramps for the background reference (black points) and the rows affected by the artifact (red points). It is clear that the frames or groups taken after the disk source saturates are not affected by the distortion of the ramp from the row effect. In fact, we have shown that fitting the portion of the ramp after saturation gives the correct flux result compared with the background reference. This result will be important for the interpretation of the effect in MRS data in Section 3.

Next, in Figure 9 we show the "pure" column and row effect on the ramps. Here we have subtracted the background reference box region from the artifact region, which removes other reset effects that affect the shape of the ramp. What is left is just the effect on the signal of the ramp from the column and row artifact, which we can see evolves from low flux (red points) to high flux (black points). Again, from this figure it is clear that the effect manifests differently for the row and column artifacts. Figure 9 shows clearly that the origin of the row and column artifact is in the

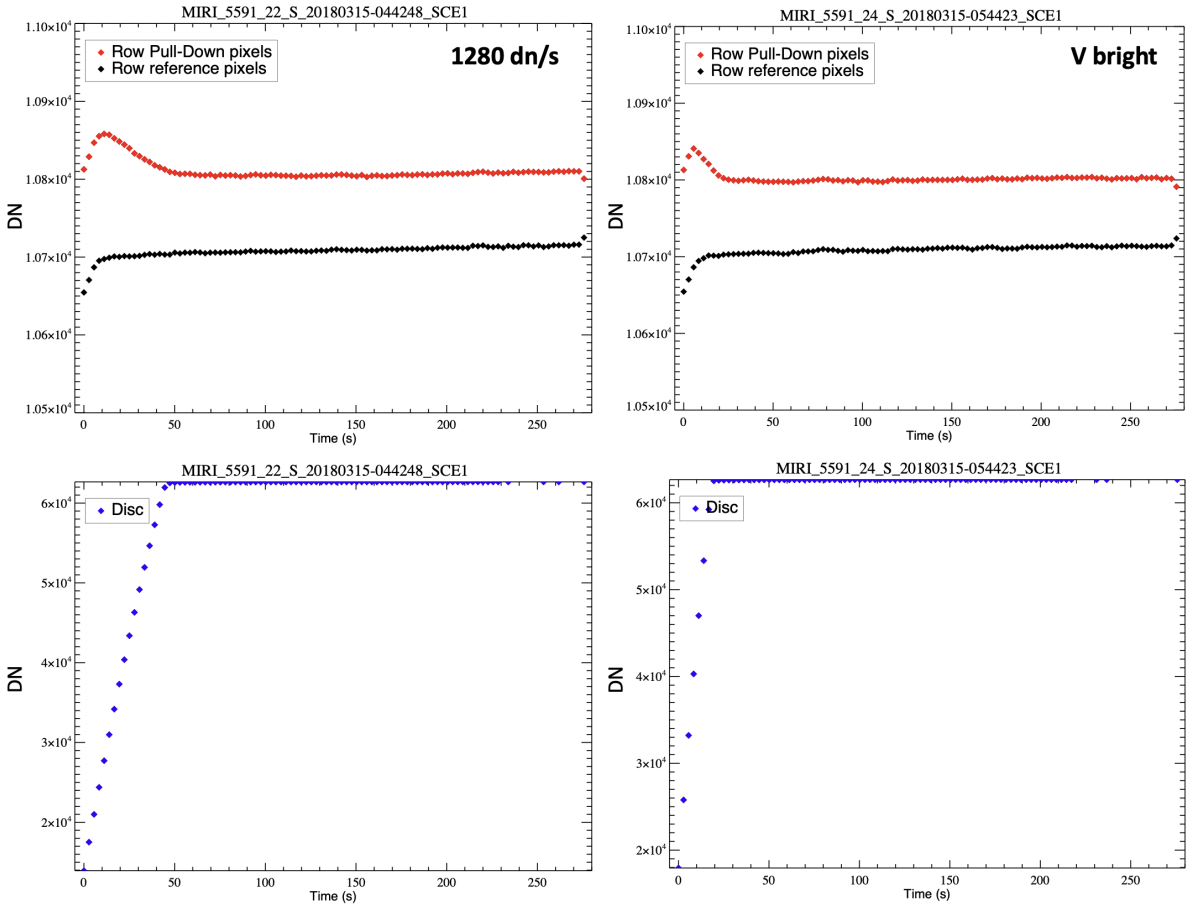

Fig 8 Identical to Figure 7 but showing results for higher flux test sources.

ramp itself and is not a simple offset in flux. Additionally, how the row-column artifacts manifest in the flux images depends strongly on how the slope is fitted on the affected ramps. The length of the ramp (i.e. number of groups) is an important factor, as a ramp with a low number of groups will have a very different slope due to the row-column artifact than a ramp with many groups. This also explains why the row-column artifacts sometimes are seen as pull-up and sometimes pull-down in the resulting flux image, both for the MIRI detectors and the Spitzer IRAC ones.

As we mentioned in Section 2 the row artifact is not just apparent in the rows in which there are sources in the JPL test images. For the more extended disc-like source in the JPL test image we see rows above the image that are also affected. To investigate this further in Figure 10 we plot

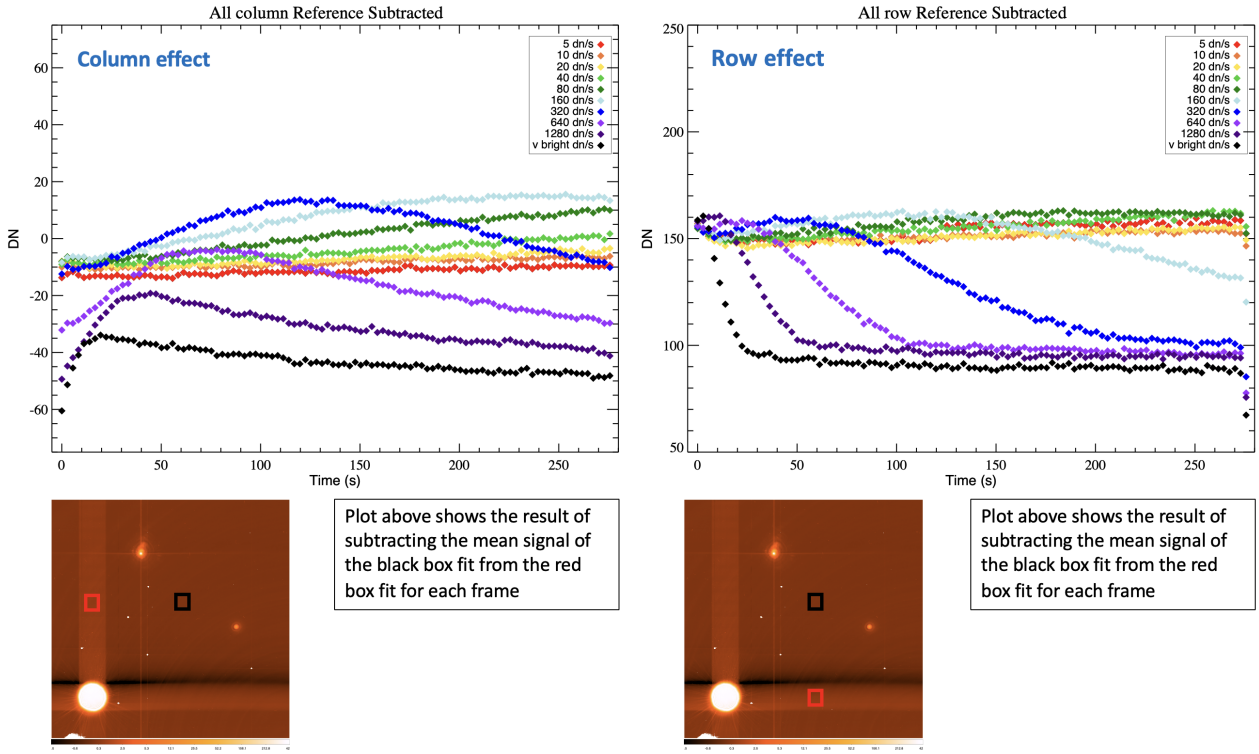

Fig 9 Showing the column and row affected ramps for many different flux levels represented by different colours in the plot. The reference background was subtracted from these ramps, frame by frame, thus removing any other reset effects that change the shape of the ramp. The result is the ”pure” row and column artifacts.

the reference-subtracted ramps for rows that span across the disk image in the JPL test from rows 100 to 280. The figure shows that after an initial increase in the ramp on the lower rows below the disk image, a strong pull down is seen in the ramp data that peaks at the top row of the disk image (around row 220). It is again interesting that the strongest row effect does not come from the rows with the most strongly illuminated pixels i.e the centre of the disc. For this extended source the strongest effect comes from the illuminated pixels at the top of the source, noting that the read direction of the detector is from bottom to top. This indicates, for the row artifact, that the effect is cumulative in the read direction for extended or resolved sources.

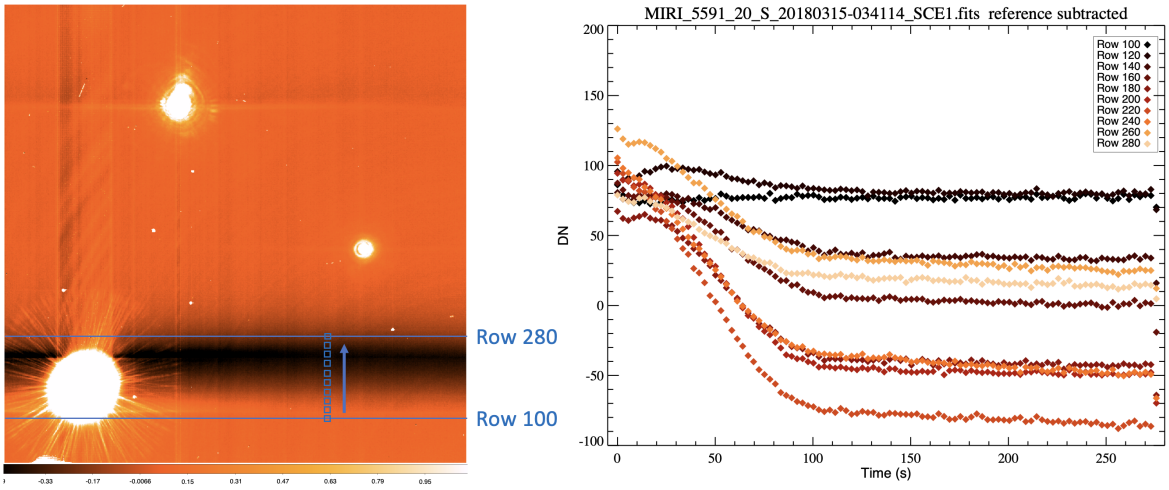

Fig 10 Investigating how the row artifacts change as we move up rows across the extended disk source. The small blue boxes in the image on the left represent the regions plotted as ramps in the right of the figure.

2.2 Further investigation at NASA JPL

During additional testing at NASA JPL the effect on the row column artifacts of adjustments to the detector bias voltages was investigated, but with no apparent change in the behaviour. We also found that there is no significant change in the effect from integration to integration i.e. all integrations[5] are affected in the same way. However, the MIRI detectors also can be read in sub-array mode.[2] In Figure 11 we show three images from a different engineering MIRI detector than used in the tests discussed so far. The set up for this detector is the same as discussed above but the mask between the black body source and the detector has a disc-like hole in the top right of the detector image and there is no 15 micron filter. The left image shows the full array with a strong row-column effect from the disk source. The middle image shows the same detector but divided into sub-array left and right while the image on the right shows the same detector image but divided into two sub-arrays top and bottom.

The striking result is that the row artifact in the middle image of Figure 11 does not cross the

[5]Integrations denote the multiple ramps per exposure - see explanation in JWST documentation.

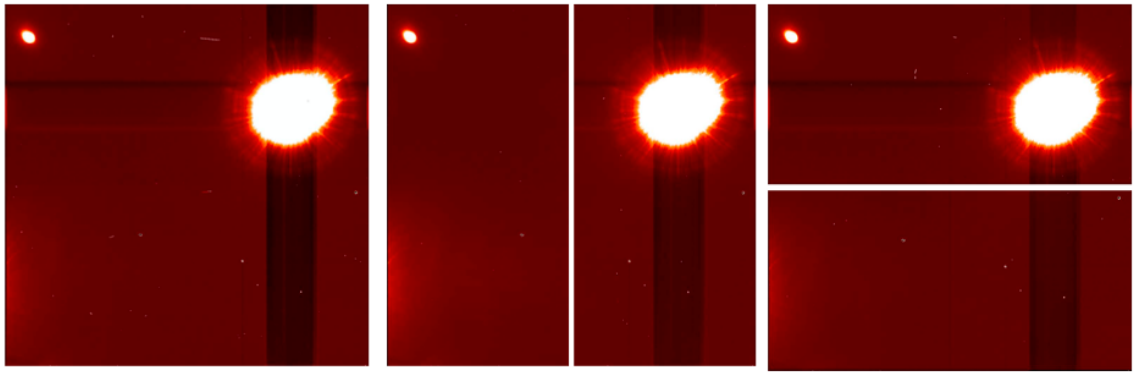

Fig 11 Right full detector image, centre same image but read in two sub-arrays – dividing image in half. Right same image but divided in two horizontal sub-arrays. All figures are scaled exactly the same.

boundaries of the sub-array when only the left hand sub-array is read out. i.e. a source outside the portion of the detector that is being read does not cause a row artifact. Oppositely though, in the right hand image of Figure 11 we see that the column effect does cross the boundary between sub-arrays i.e. when only the bottom sub-array is readout you still see the column artifact. Therefore a source outside of the sub-array can create a column artifact in the sub-array being read but not a row artifact. This result has consequences for MRS and coronagraphic imaging as discussed in Section 6 and 7.

3 Row-Column Effect in the MIRI MRS

While working on row-column issue in JPL test data, which relates more logically to MIRI imaging, in parallel the effect was found in ground tests with MIRI's Medium Resolution Spectrometer (MRS). In the MRS data it was noticed that there was a strange tick shape (or check mark) in the low flux data for ramps in band 4C of the MRS. Figure 12 shows the mean ramp and slope results of all pixels in slices for the MRS Channel 4.

With closer inspection the check mark data look similar to the row effect we see for bright sources in the JPL tests, e.g., the right hand plot of Figure 8. We therefore identified the problem

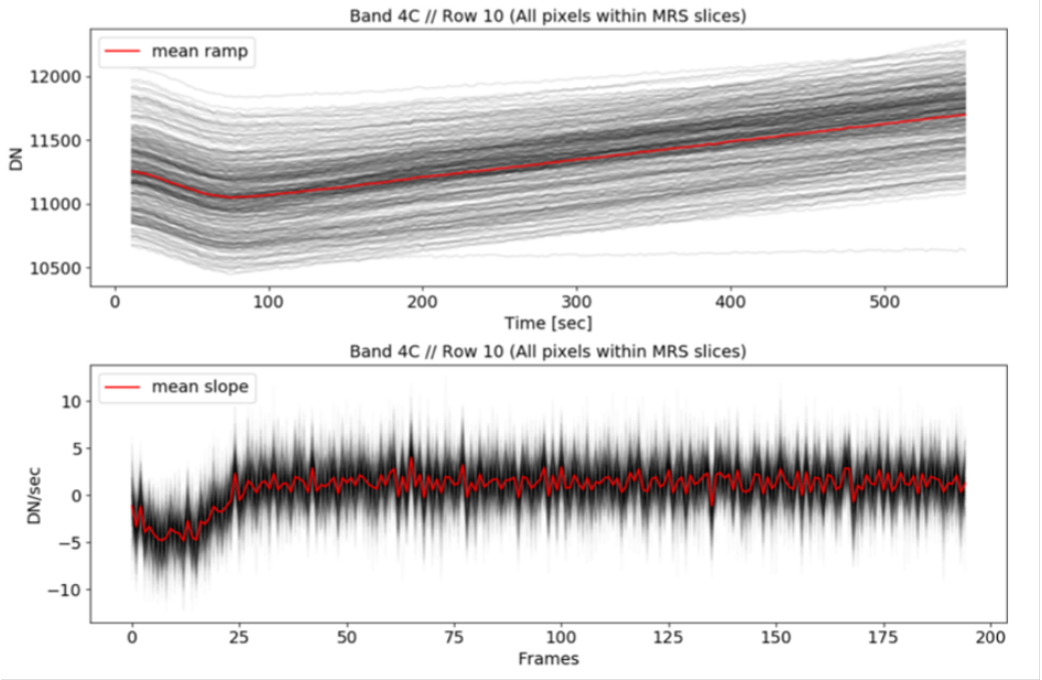

Fig 12 Mean ramp and slope results showing a strange uptick (ramp) or dip (slope) in the band 4C data.

as due to the row effect. In the case of the MRS, two spectral channels are always imaged on a detector plane. In the case of MRS band 4C, the band is imaged on the left half of the detector, and band 3C is imaged on the right half of the detector (see Figure 13). There is a large signal contrast between the pixels on each side. This is mainly due to a significantly lower quantum efficiency at around 28 microns in Channel 4 compared to 17 microns in Channel 3 for these data. The detector layout is shown in Figure 13 where we identify the location of the uptick in the ramp that led to the discovery of the row-column artifacts in the MRS data.

It is important that, although the row effect was identified in data where the adjacent Channel 3 data was saturated, we can expect that the effect of the brighter Channel 3 data on Channel 4 will exist at all flux levels of the brighter Channel. Figure 9 also shows that lower fluxes, that do not saturate, may have a greater effect on the Channel 4 ramps, since the whole of the ramp may be distorted by the brighter Channel 3 signal, rather than just the beginning as shown in this example

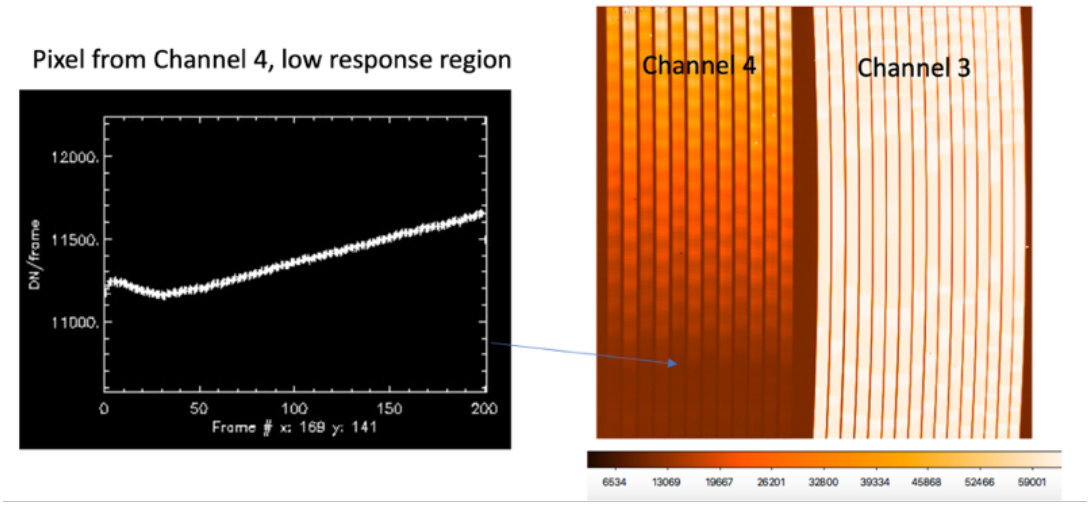

Fig 13 Showing an example of a pixel in Channel 4 that shows the uptick. Note that Channel 3 is saturated.

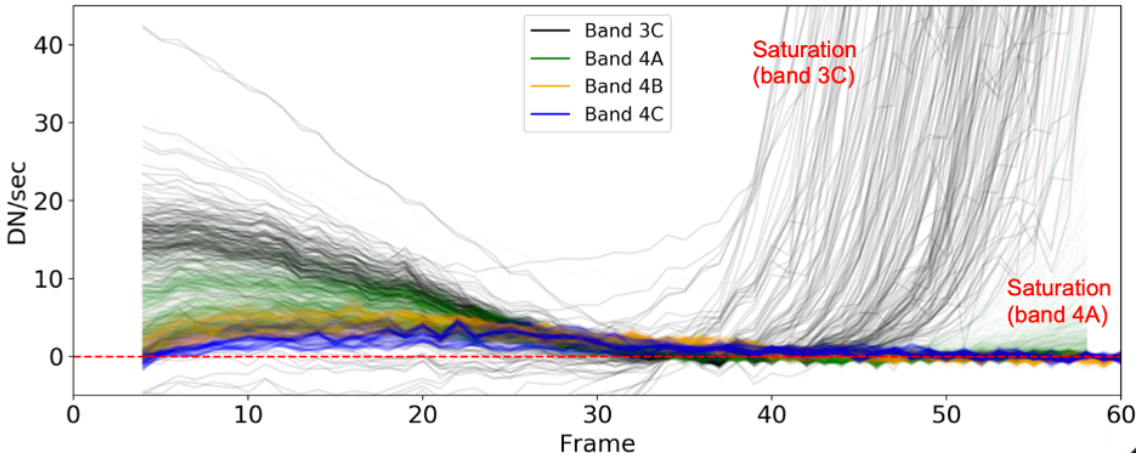

Fig 14 Showing an example of a pixel in Channel 4 that shows the uptick. Note that Channel 3 is saturated.

data set in Figure 12. Evidence for this dependence of the effect on flux in the MRS can be seen in Figure 14 where we show the residuals of a linear fit to unaffected frames after saturation to the row-affected data in the MRS. A clear trend in the effect residuals can be seen between the different bands.

Given the row effect for the MRS data, it seems likely that the column effect might also be present in MRS data, as the detector/multiplexer technology is identical across all MIRI modes. The difference is that different wavelengths, dispersed by the MRS diffraction gratings, are pro-

jected in the detector column direction (see again Figure 13) and so, unlike the imager, there are no un-illuminated regions in the column direction. This may mean that any column effect is of little concern, although we note that the MRS slices are not perfectly collimated in the x pixel direction with detector pixels i.e. they are curved. However, because the row-column effect appears when there is high flux contrast between regions of the detector, and there is little high contrast in the MRS slices in the column direction, it is thought that the column effect will have little impact in most science cases. An extreme science case to keep in mind is that of a bright/saturated spectral emission line on a weak spectral continuum.

4 Row-Column Effect in MIRI Imager Flight Data

Finding evidence for row and column effect in MIRI imager flight data has proved more difficult than for ground test data. In the first instance JWST is so sensitive that the many detected sources make it difficult to pick out the artifacts, see Figure 15 as an example. Moreover, for MIRI at wavelengths up to 10 microns the PSF includes a cruciform feature in the x and y detector pixel directions that stretches for hundreds of pixels.[8] This cruciform artifact will mix with any row or column artifact for bright point sources making it difficult to distinguish between them. Additionally, we also expect that the higher flight backgrounds will dilute the row-column effects making them harder to see, because this reduces the contrast between the background and the astronomical sources. For these reasons it is almost impossible to see the artifacts in the flux image of individual MIRI imaging pointings (i.e. one dither); instead, we have to look to images combining dithered data to have enough signal to noise on the background to see the artifacts.

Figures 15 and 16 show MIRI flight images (Pipeline Level 2a) for the bright spectral calibration nebula SMP-LMC-58 at 5.6 and 12.8 microns respectively. The first thing to note is that the

column and row artifacts are hardly visible in the two images until we stretch the background. This means that the artifact in flight data still has the same very low amplitude flux change on the ramp as we saw in ground test data - typically a few tenths of a DN/s in signal.

In the right hand image for Figures 15 and 16, where the background is stretched, we can see column artifacts as well as a row artifact at 12.8 microns. At 5.6 microns we see columns for the bright nebula as well as some of the stars in the image, but at 12.8 microns we only see column artifacts for the bright nebula. This is likely because the background is higher at 12.8 microns, reducing the contrast, and the spectral energy distributions of stars fall toward longer wavelengths contrary to the behavior of the bright nebula.

The fact that we do not see obvious row artifacts in the 5.6 micron image can be explained by the fact that the bright nebula saturates in less than 3 frames for this 17 group data set. And as we know from ground testing the row artifact distortion disappears in the ramp after the source saturates. This means the row artifact should have a reduced impact on the ramp, especially because the pipeline rejects the first 2 frames as part of the reset switch charge decay (RSCD) correction step.

A row artifact is much more apparent at 12.8 microns. This is because the number of pixels that saturate is increased at 12.8 microns as the PSF core is larger. Also, in line with the MIRI detector physics, there is no expected cruciform part to the PSF at 12.8 microns making it easier to distinguish the row effect.

Finally, one difference with ground test data and Spitzer IRAC is that the column artifact in flight data appears different above and below the source of origin. This is particularly clear in Figure 16 as well as Figure 22 below. At the time of writing we do not have a good explanation for the difference but it may be connected to the influence of the row artifact on the column artifact in

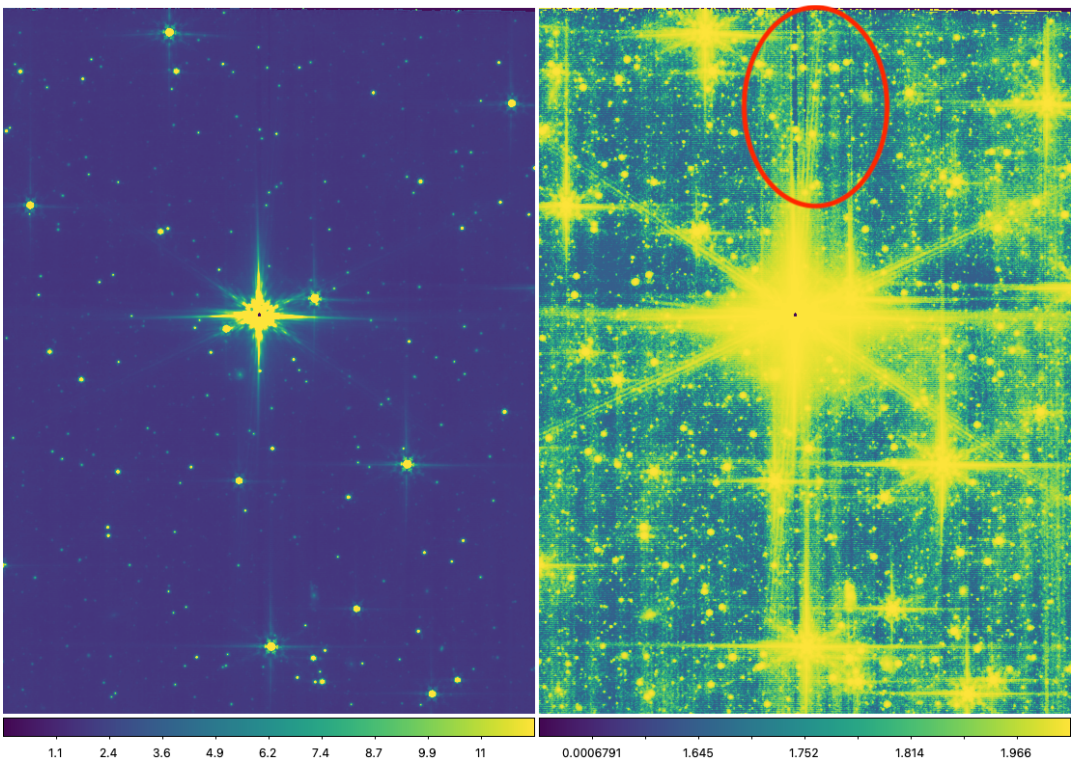

Fig 15 Showing a MIRI commissioning image at 5.6 μm of the spectral calibration nebula SMP-LMC-58, taken as part of program ID 1090. The left image is at a typical stretch; the centre of the nebula is saturated and the cruciform artifact is prominent. The right image is identical but with the background cut stretched to reveal the column artifacts from the nebula and other bright stars in the image, circled in red.

the read direction up the detector.

5 Row-Column Effect in MIRI MRS Flight Data

For the MRS we begin by confirming the presence of the row artifact that was apparent in ground testing from data taken with the onboard calibration lamp. Similar calibration lamp data sets were taken in commissioning where we show the detector image in Figure 17. The resulting slopes of the band 4C data that are affected by the saturating band 3C data are shown in Figure 18 alongside the ground data results. Although there is a slight offset between the ground and flight data, the characteristic check mark shape tells us that the row effect is still present in this data set.

Looking next at on-sky data for MIRI's MRS, in Figure 19 we show the detector image from

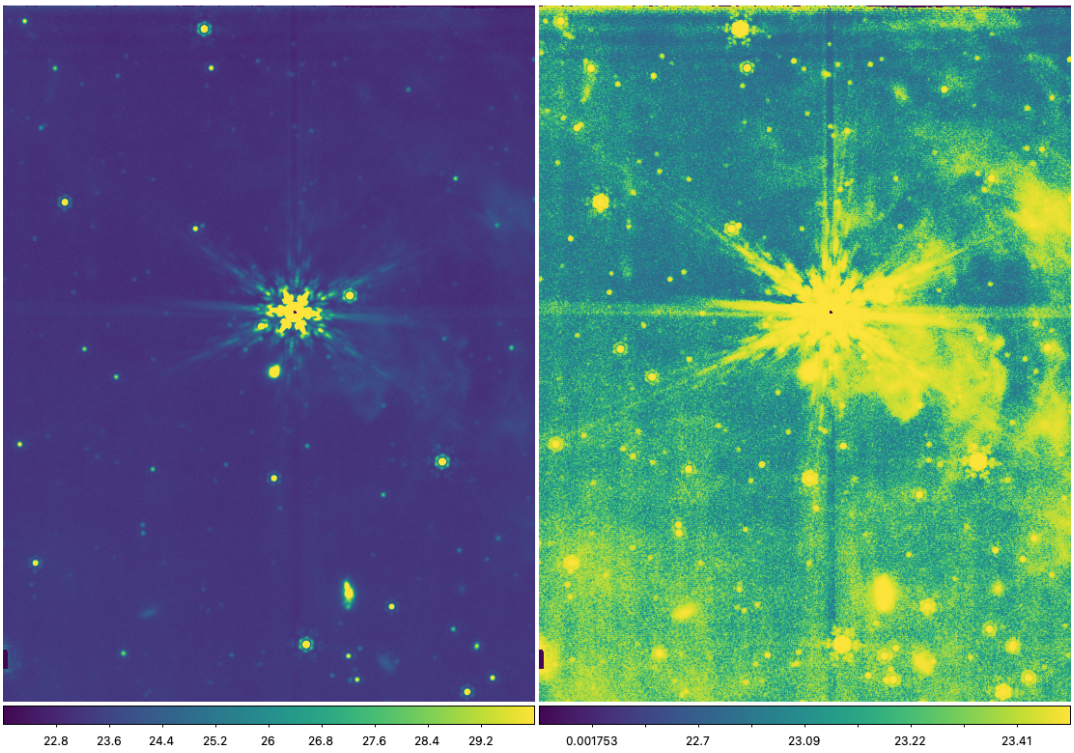

Fig 16 Showing the MIRI commissioning image at 12.8 μm of the spectral calibration nebula SMP-LMC-58. The left image shows that the centre of the nebula is saturated and the cruciform is virtually absent at this wavelength; the right image is identical but with the background cut stretched to reveal the column and row artifacts.

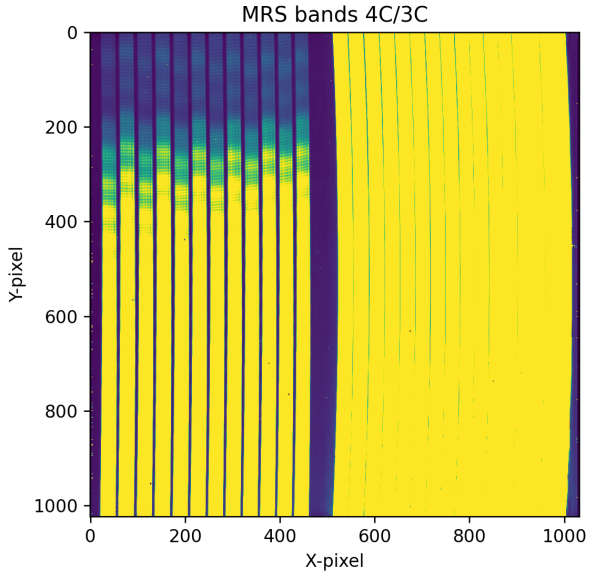

Fig 17 Showing the detector image for MIRI MRS commissioning internal calibration lamp data. The bright Channel 3C is on the right and the fainter Channel 4C on the left.

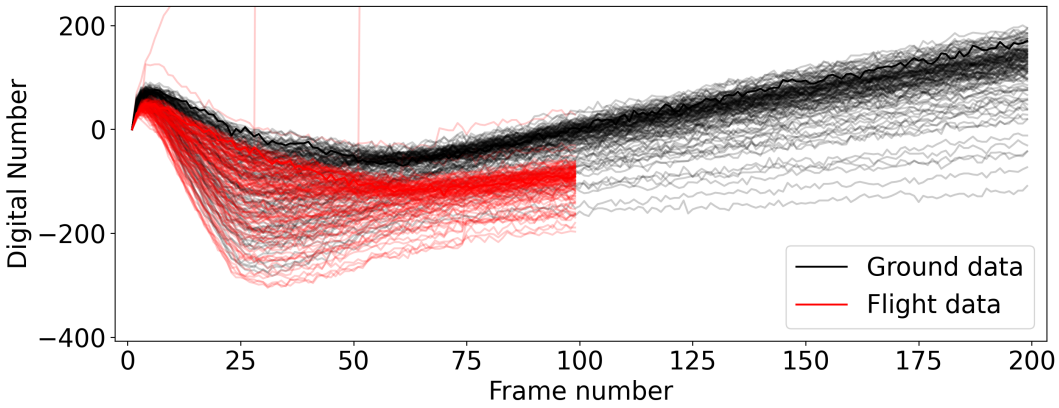

Fig 18 Showing the ramps in Band 4C of the MIRI MRS that are affected by the saturation of the data in Band 3C. Here we compare ground and flight test results.

an observation of the bright Cat's Eye Nebula (NGC-6543, Program ID 1047), again for Bands 4C/3C. The nebula has bright emission lines at the bottom of band 3C (on the right). To see if the bright emission lines have an effect on the 4C band we can look at the gap region between the two bands on the detector. In Figure 20 we have plotted the ramps from two pixels in the gap region: (1) one in the same row as the bright emission line shown in orange and (2) another in a row above the emission lines. Figure 20 clearly shows a distortion to the ramp in the first case, confirming the row artifact in flight MRS data.

6 Impacts

6.1 MIRI imaging

Pre-launch we expected that the primary factor when considering the impact of the row and column artifact for imaging is the level of background. As mentioned above, the low background environment of the JPL test bed allows for a clear study of the artifacts but flight backgrounds are at least 3 times higher than the ground test data. Flight data have shown that the backgrounds do indeed reduce the prominence of row column artifacts seen in imaging as relatively high backgrounds in

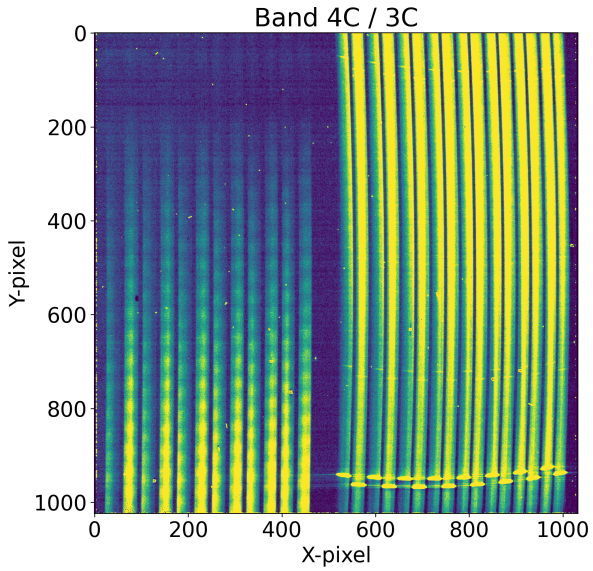

Fig 19 Showing the detector image for an MRS observation of the bright Cat's Eye Nebula (NGC-6543) - Bands 4C/3C

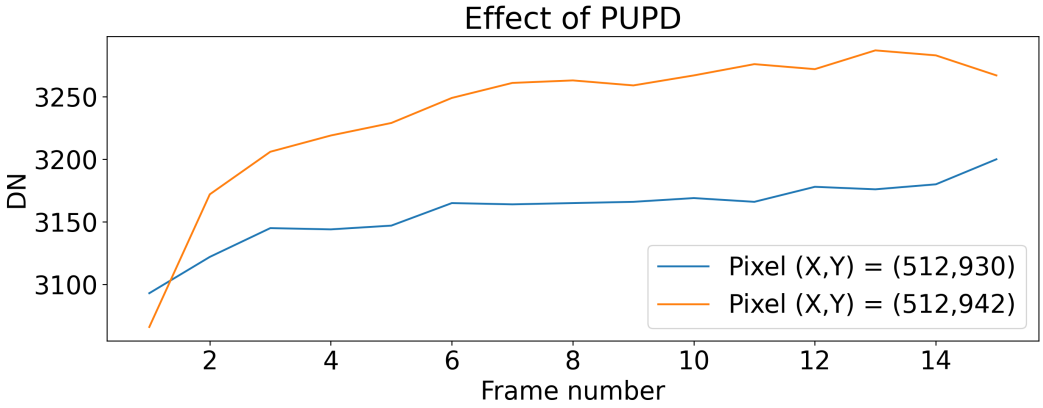

Fig 20 Plotting the ramps from two pixels in the gap region between the two long wavelength bands 3C and 4C of the MRS. The orange ramp is for a pixel in the row of a bright emission line in band 3C and the blue ramp is for a pixel without a bright line.

flight reduce the contrast between the source and background. However, real flight sources are also a lot brighter than our ground test sources so we will still see row column artifacts at all levels of background. How the row and column effects impact MIRI imaging is heavily dependent on the length of the ramp and the rate at which the bright source saturates. With further study it may be possible to predict the row and column impact for a certain flux and ramp length.

6.2 MIRI medium resolution spectroscopy

For the MRS one impact is clear: a bright Channel will affect a faint Channel as they are observed side by side on the detector, as discussed above. The Channel 3C influence on Channel 4C is the primary situation where a strong artifact in the ramps might occur; whenever Channel 3C is saturated, the data in Channel 4C is affected. However, the effect is present at all flux levels for low backgrounds so it may be important also for the shorter wavelength Channels 1 and 2 as well as bands A and B for all Channels within their full wavelength range.

The column effect in the MRS is harder to characterise; however, as discussed above, in the first instance the effect is not as important since there is no unilluminated science region in the column direction for the MRS and, secondly, the flux contrast in the y direction, up and down a slice, is low.

6.3 MIRI LRS and coronagraphs

Row-column artifacts have not yet been identified in the MIRI Low Resolution Spectrograph (LRS) or the MIRI coronagraphs. However, they share the same detectors as the MIRI imager and MRS so some impact from row-column artifacts is expected.

For the LRS a possible source of row-column artifacts could be a bright source in the imager

field of view that causes row artifacts in the LRS spectrum, which is dispersed behind a mask but not isolated electrically from the rest of the detector array. Column artifacts could also be created from bright spectral lines.

For the coronagraphs, the images are taken in sub-array mode so they will not be affected by bright targets in the imager field of view, because we have shown that the row artifact does not appear when the source is out of the sub-array. However the coronagraphs could and probably will suffer from column artifacts from bright sources out of the sub-array field of view. We have already seen column artifacts from bright cosmic rays on the sub-array in coronagraph imaging. Bright stars within the coronagraph sub-array could also cause issues, for example a close binary star is a case that has been discussed in Beichman et al. (2020).[9]

7 Correction

At the time of writing there is no JWST pipeline correction for row-column artifacts in MIRI data. A correction was investigated pre-flight, but it was thought that the flight performance needed to be known before any correction could be developed further. However, we now know the effect is still present in flight data, perhaps somewhat surprisingly, even in high background long wavelength MIRI imaging. Therefore the MIRI instrument team is in the process of developing a correction as a pipeline tool with the idea that it could be included in a future optimized version of the JWST pipeline.

7.1 Optimal pipeline correction for imaging

Because Spitzer's IRAC instrument shares similar multiplexers and the same type of detectors as MIRI (Si:As BIB) one starting point for a correction for MIRI imaging can be based on the column-

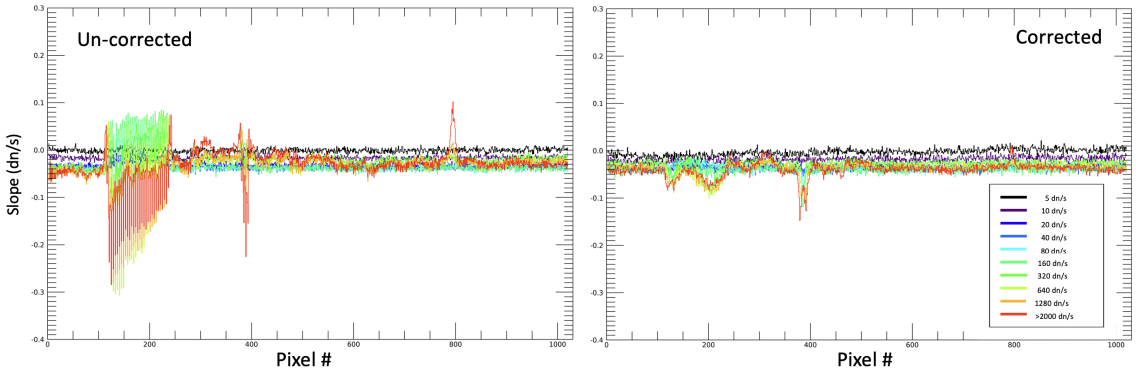

Fig 21 Plots showing median profile correction to JPL ground test data. Left is the original profiles, where the colours represent different flux levels of the black body test source. Right shows the corrected profile.

row correction used for that instrument (https://irsa.ipac.caltech.edu/data/SPITZER/docs/irac/features/#2B). As Spitzer did not have the frame or ramp data available, the correction had to be done on the slope image. The basis of the correction for IRAC was to mask the objects of interest and calculate a median row and column value that was projected and compared to the actual row and column to identify outliers. Then using thresholds the results were used to correct the image.

Along the same lines as the IRAC solution we made an initial attempt at correcting the row and column artifacts in the JPL ground test data presented in Section 2. Figure 21 shows the results. Firstly we created a median profile from source free columns, in this case from columns 900 to 1000. Then we inverted the median profile and subtracted it from all the columns. Figure 21 shows that we managed to reduce the impact of the artifact by approximately an order of magnitude.

We also tried a variation of this simple median profile correction on flight images again showing promising results as applied to the Early Release Observation of Stephan's Quintet (Program ID 2732). Here the column and row profiles were constructed and applied independently, above/below and left/right of very bright sources visually showing this effect. An example of the correction application is shown in Figure 22. This correction is not yet available in the pipeline.

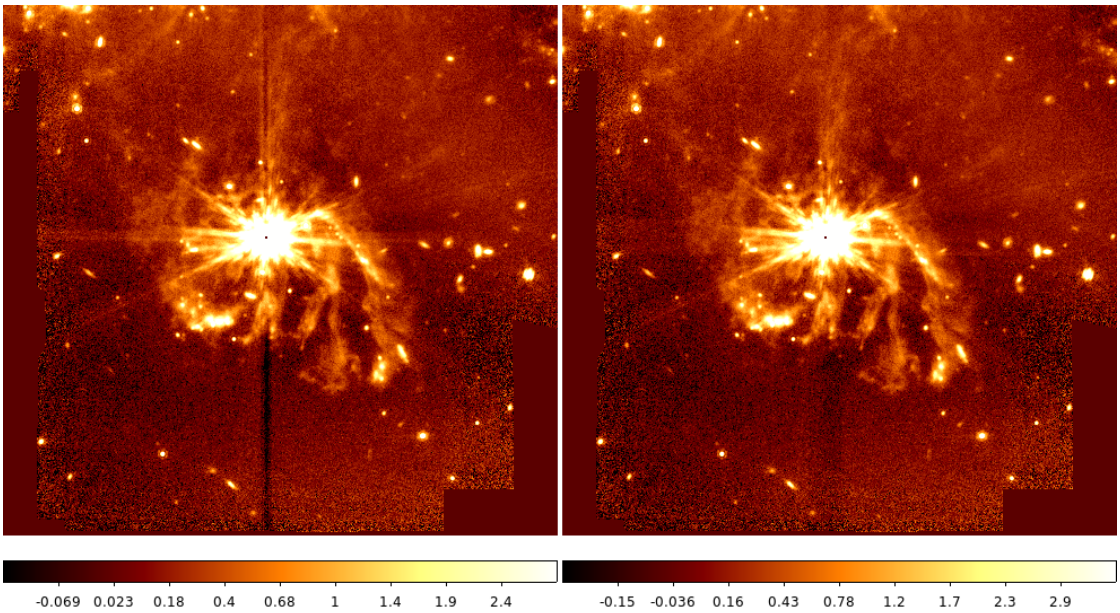

Fig 22 MIRI imaging data of a galaxy in Stephan's Quintet (Program ID 2732). Column and row artifacts in the left image are cleaned in the right image by the subtraction of median row and column profiles.

7.2 Row correction in the MRS

The MRS benefits from interslice regions as well as inter Channel regions of the detector. As shown in Figure 23 the inter Channel region can be used to measure the row effect of the row artifact on the ramp from the bright Channel to the less bright Channel.

Figure 24 demonstrates how the inter Channel region could be used for a basic correction method for an MRS science pixel in band 4C. The corrected ramp of the science pixel is derived by subtracting from it the ramp of the nearest non-science pixel. The empirical method is promising given that the slope of the frames impacted by the row-column effect agrees with the rest of the ramp.

8 Summary

Row and column artifacts that are associated with bright sources in MIRI imaging and Medium Resolution Spectrometer have been observed in ground testing and flight data. The main results of

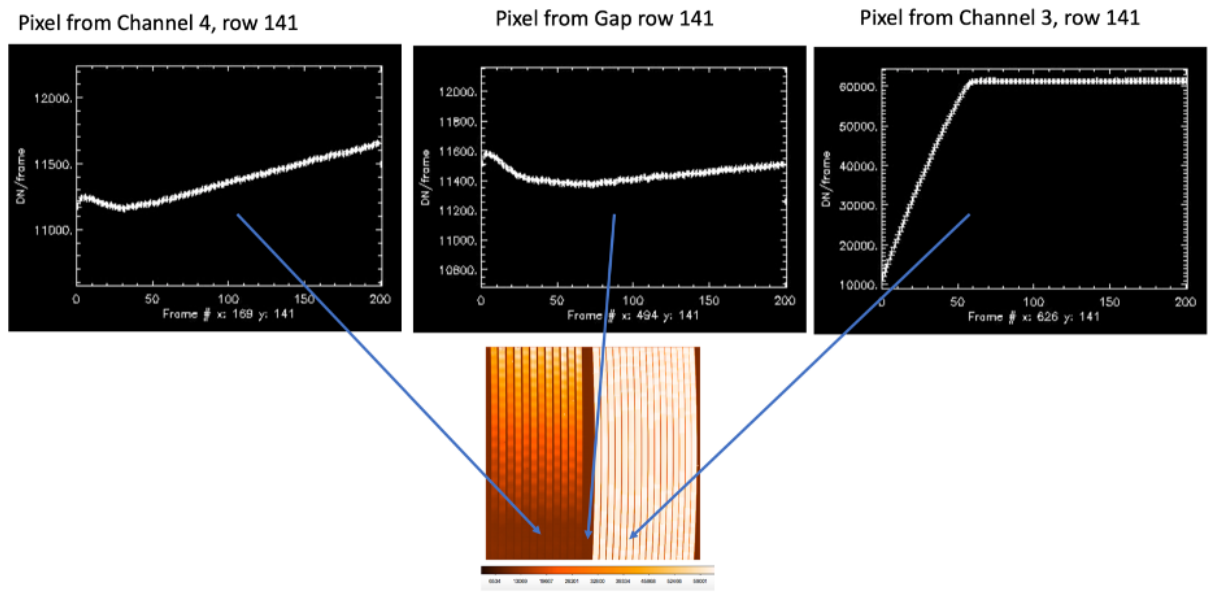

Fig 23 Showing the ramps from three regions of the MRS, Channel 4C, Channel gap, Channel 3C.

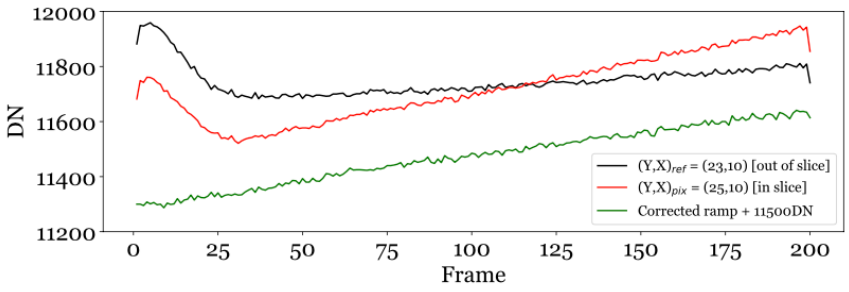

Fig 24 Example of inter Channel correction of the ramp.

the characterisation of the row and column artifacts are summarised here:

- The row and column artifacts are present at all levels of illumination – however they are most prominent when the observed source is at high contrast compared to the background.
- The effect was first identified in slope images but is actually due to a change in the shape of the ramp which is in turn dependent on the frame in which the integration ramp saturates.
- The column artifact is only apparent in columns that include bright sources whereas the row effect is also seen in rows above those that include the sources.
- For row affected pixels the effect in the ramp disappears when the illuminated pixels causing the effect saturate.
- For pixels that show the column artifact the ramp is seen to go negative at the point in which the signal saturates.
- Because it is an effect that changes the shape of the ramp, the way the ramp is fitted will affect the resulting slope images i.e. short ramps or long will give different results.
- The absolute peak flux of the pixels seems to be more dominant in the effect than the number of pixels illuminated in any row or column.
- The effect is identical in the ramps of all multiple integration data.
- The row and column effects do not seem to have the same origin and have different characteristics – notably the row effect does not cross sub-array boundaries (i.e. objects outside the sub-array field of view do not have an influence) where the column effect does.

- The flight column artifact appears to have different strengths above and below the source or origin, contrary to the results of ground testing and the IRAC effect where the artifact was symmetric. This issue is still under investigation.

- Pipeline solutions for the row and column effects are under development for the imager and MRS showing promising results.

References

1 G. H. Rieke, M. E. Ressler, J. E. Morrison, *et al.*, "The Mid-Infrared Instrument for the James Webb Space Telescope, VII: The MIRI Detectors," *PASP,* **127**, 665 (2015).

2 M. E. Ressler, K. G. Sukhatme, B. R. Franklin, *et al.*, "The Mid-Infrared Instrument for the James Webb Space Telescope, VIII: The MIRI Focal Plane System," *PASP,* **127**, 675 (2015).

3 A. Mainzer, M. Larsen, M. G. Stapelbroek, *et al.*, "Characterization of flight detector arrays for the wide-field infrared survey explorer," in *High Energy, Optical, and Infrared Detectors for Astronomy III*, D. A. Dorn and A. D. Holland, Eds., *Society of Photo-Optical Instrumentation Engineers (SPIE) Conference Series* **7021**, 70210X (2008).

4 J. D. Mill, R. R. O'Neil, S. Price, *et al.*, "Midcourse space experiment: Introduction to the spacecraft, instruments, and scientific objectives," *Journal of Spacecraft and Rockets* **31**, 900–907 (1994).

5 T. Onaka, H. Matsuhara, T. Wada, *et al.*, "The Infrared Camera (IRC) for AKARI – Design and Imaging Performance," *PASP,* **59**, S401 (2007).

6 J. L. Hora, G. G. Fazio, L. E. Allen, *et al.*, "In-flight performance and calibration of the Infrared Array Camera (IRAC) for the Spitzer Space Telescope," in *Optical, Infrared, and Millime-*

ter Space Telescopes, J. C. Mather, Ed., *Society of Photo-Optical Instrumentation Engineers (SPIE) Conference Series* **5487**, 77–92 (2004).

7 J. L. Pipher, C. W. McMurtry, W. J. Forrest, *et al.*, "Comparison of laboratory and in-flight performance of infared array camera (IRAC) detector arrays on Spitzer Space Telescope," in *Optical, Infrared, and Millimeter Space Telescopes*, J. C. Mather, Ed., *Society of Photo-Optical Instrumentation Engineers (SPIE) Conference Series* **5487**, 234–243 (2004).

8 A. Gáspár, G. H. Rieke, P. Guillard, *et al.*, "The Quantum Efficiency and Diffractive Image Artifacts of Si:As IBC mid-IR Detector Arrays at 5-10 μm: Implications for the JWST/MIRI Detectors," *PASP,* **133**, 014504 (2021).

9 C. Beichman, M. Ygouf, J. Llop Sayson, *et al.*, "Searching for Planets Orbiting α Cen A with the James Webb Space Telescope," *PASP,* **132**, 015002 (2020).

List of Figures

3 Showing the row artifact profiles in a flux image. The profiles for four different flux levels are plotted, which correspond to the profile as represented by the red line in the inset image.

4 Showing flux images from NASA JPL test bench. The row-column artifact can be seen to have a stronger influence as the flux of the source increases.

5 Showing the flux image from the JPL test bench. The three boxes mark regions used in the following investigation. The black box marks a region used as a reference background. The red box marks a region used to investigate an area with row or column artifacts. The blue box represents a region on the JPL test source image itself. The disk source is used in the following investigation

6 Showing four plots, each one for a different flux level in the JPL test, where the source flux was set to 80, 160, 320 and 640 DN/s. The detector outputs are color-coded to match the color of the relevant box in Figure 5. The black points represent the signal measured from an individual frame of the ramp in the reference region as defined in Figure 5. The red points represent the same measurement per frame for the column artifact region. The blue points show the signal from the disk test source itself.

7 Same as for Figure 6 but the red points here show the signal in individual frames or the ramp for the row artifact.

8 Identical to Figure 7 but showing results for higher flux test sources.

9 Showing the column and row affected ramps for many different flux levels represented by different colours in the plot. The reference background was subtracted from these ramps, frame by frame, thus removing any other reset effects that change the shape of the ramp. The result is the ”pure” row and column artifacts.

10 Investigating how the row artifacts change as we move up rows across the extended disk source. The small blue boxes in the image on the left represent the regions plotted as ramps in the right of the figure.

11 Right full detector image, centre same image but read in two sub-arrays – dividing image in half. Right same image but divided in two horizontal sub-arrays. All figures are scaled exactly the same.

12 Mean ramp and slope results showing a strange uptick (ramp) or dip (slope) in the band 4C data.

13 Showing an example of a pixel in Channel 4 that shows the uptick. Note that Channel 3 is saturated.

14 Showing an example of a pixel in Channel 4 that shows the uptick. Note that Channel 3 is saturated.

15 Showing a MIRI commissioning image at 5.6 μm of the spectral calibration nebula SMP-LMC-58, taken as part of program ID 1090. The left image is at a typical stretch; the centre of the nebula is saturated and the cruciform artifact is prominent. The right image is identical but with the background cut stretched to reveal the column artifacts from the nebula and other bright stars in the image, circled in red.

16 Showing the MIRI commissioning image at 12.8 μm of the spectral calibration nebula SMP-LMC-58. The left image shows that the centre of the nebula is saturated and the cruciform is virtually absent at this wavelength; the right image is identical but with the background cut stretched to reveal the column and row artifacts.

17 Showing the detector image for MIRI MRS commissioning internal calibration lamp data. The bright Channel 3C is on the right and the fainter Channel 4C on the left.

18 Showing the ramps in Band 4C of the MIRI MRS that are affected by the saturation of the data in Band 3C. Here we compare ground and flight test results.

19 Showing the detector image for an MRS observation of the bright Cat's Eye Nebula (NGC-6543) - Bands 4C/3C

20 Plotting the ramps from two pixels in the gap region between the two long wavelength bands 3C and 4C of the MRS. The orange ramp is for a pixel in the row of a bright emission line in band 3C and the blue ramp is for a pixel without a bright line.

21 Plots showing median profile correction to JPL ground test data. Left is the original profiles, where the colours represent different flux levels of the black body test source. Right shows the corrected profile.

22 MIRI imaging data of a galaxy in Stephan's Quintet (Program ID 2732). Column and row artifacts in the left image are cleaned in the right image by the subtraction of median row and column profiles.

23 Showing the ramps from three regions of the MRS, Channel 4C, Channel gap, Channel 3C.

24 Example of inter Channel correction of the ramp.